TISSUE ENGINEERING: Part A
Volume 20, Numbers 9 and 10, 2014
© Mary Ann Liebert, Inc.
DOI: 10.1089/ten.tea.2013.0438

Hypertensive Rat Lungs Retain Hallmarks of Vascular Disease upon Decellularization but Support the Growth of Mesenchymal Stem Cells

Michelle E. Scarritt, BS,[1] Ryan W. Bonvillain, PhD,[1] Brian J. Burkett, MS,[1] Guangdi Wang, PhD,[2] Elana Y. Glotser, MS,[2] Qiang Zhang, MD,[2] Mimi C. Sammarco, PhD,[3] Aline M. Betancourt, PhD,[1,4] Deborah E. Sullivan, PhD,[1,4] and Bruce A. Bunnell, PhD[1,5]

There are an insufficient number of donor organs available to meet the demand for lung transplantation. This issue could be addressed by regenerating functional tissue from diseased or damaged lungs that would otherwise be deemed unsuitable for transplant. Detergent-mediated whole-lung decellularization produces a three-dimensional natural scaffold that can be repopulated with various cell types. In this study, we investigated the decellularization and initial recellularization of diseased lungs using a rat model of monocrotaline-induced pulmonary hypertension (MCT-PHT). Decellularization of control and MCT-PHT Sprague-Dawley rat lungs was accomplished by treating the lungs with a combination of Triton X-100, sodium deoxycholate, NaCl, and DNase. The resulting acellular matrices were characterized by DNA quantification, Western blotting, immunohistochemistry, and proteomic analyses revealing that decellularization was able to remove cells while leaving the extracellular matrix (ECM) components and lung ultrastructure intact. Decellularization significantly reduced DNA content ($\sim$30-fold in MCT-PHT lungs and $\sim$50-fold in the control lungs) and enriched ECM components ($>$60-fold in both the control and MCT-PHT lungs) while depleting cellular proteins. MicroCT visualization of MCT-PHT rat lungs indicated that the vasculature was narrowed as a result of MCT treatment, and this characteristic was unchanged by decellularization. Mean arterial vessel diameter of representative decellularized MCT-PHT and control scaffolds was estimated to be 0.152 ± 0.134 mm and 0.247 ± 0.160 mm, respectively. Decellularized MCT-PHT lung scaffolds supported attachment and survival of rat adipose-derived stem cells (rASCs), seeded into the airspace or the vasculature, for at least 2 weeks. The cells seeded in MCT-PHT lung scaffolds proliferated and underwent apoptosis similar to control scaffolds; however, the initial percentage of apoptotic cells was slightly higher in MCT-PHT lungs ($2.79 \pm 2.03\%$ vs. $1.05 \pm 1.02\%$ of airway-seeded rASCs, and $4.47 \pm 1.21\%$ vs. $2.66 \pm 0.10\%$ of vascular seeded rASCs). The ECM of cell-seeded scaffolds showed no signs of degradation by the cells after 14 days in culture. These data suggest that diseased hypertensive lungs can be efficiently decellularized similar to control lungs and have the potential to be recellularized with mesenchymal stem cells with the ultimate goal of generating healthy, functional pulmonary tissue.

Introduction

There are not enough donor lungs available to meet the incredible demand for lung transplantation. As of June 2013, there were over 1735 patients in the United States in need of lung transplantation; in 2012, 224 patients died while waiting for a suitable transplant and 194 patients became too sick to undergo transplantation.[1] Most lung donations are obtained from brain-dead donors; unfortunately, these lungs are highly susceptible to injury via trauma, resuscitation or ventilator-associated injury, pulmonary edema, aspiration of blood or gastric fluids, or infection—all of which render the lung unsuitable for transplant.[2] Since strict criteria reduce the number of potential donations, only 15–25% of available lungs are suitable for transplantation.[3] Moreover, lung transplant recipients require life-long immunosuppression to prevent the onset of organ rejection, and the median post-transplant

[1]Center for Stem Cell Research and Regenerative Medicine, Tulane University School of Medicine, New Orleans, Louisiana.
[2]RCMI Cancer Research Program, Xavier University of Louisiana, New Orleans, Louisiana.
[3]Department of Cell and Molecular Biology, Tulane University, New Orleans, Louisiana.
Departments of [4]Microbiology and Immunology and [5]Pharmacology, Tulane University School of Medicine, New Orleans, Louisiana.

survival time is only ~5.7 years.[3] A novel means for acquiring transplant-suitable lungs and reducing postoperative complications is crucial.

The rapidly evolving field of whole-organ decellularization holds great promise for producing bioartificial, transplant-suitable organs in the laboratory for human clinical application. Detergent-mediated whole-organ decellularization generates a three-dimensional (3D) extracellular matrix (ECM) scaffold of the organ that is apt for tissue engineering of patient-specific tissue. Because the decellularization process removes cells and cellular antigens responsible for immune rejection, organs recellularized with autologous cells have reduced risk of rejection upon transplantation. Advancing this technology to human clinical use would provide an alternative therapeutic avenue, significantly reduce the demand for transplantable organs, and decrease the organ transplant wait-list time. Scientists have reported successful decellularization and organ repopulation in the heart, liver, and kidney.[4–7] A growing number of groups have reported similar success in the lung using naïve rodent models[8–12] and, recently, in our own laboratory using rhesus macaque lungs.[13] Two groups transplanted crude bioartificial rat lungs that demonstrated short-term pulmonary function *in vivo*; however, these studies utilized either A549 carcinoma cells or freshly isolated pulmonary cells from fetal or neonatal rats to repopulate acellular rat lung matrices.[8–10,14] These studies offer essential proof-of-concept in naïve rodent models; however, to advance this technology toward increasing the availability of human transplant-suitable organs in the clinic, future research should focus on the potential regeneration of damaged, diseased, or otherwise unsuitable lungs. Herein, a more comprehensive assessment of decellularization–recellularization technology is presented using a rodent model of pulmonary disease.

Pulmonary hypertension (PHT) is a disease characterized by increased pulmonary vascular resistance, which ultimately leads to right heart failure and death.[15] Pathology of PHT includes endothelial dysfunction, proliferation of endothelial and pulmonary arterial smooth muscle cells, intimal hyperplasia and fibrosis, medial hypertrophy, and excessive metalloprotease activity in the vascular adventitia.[15–17] PHT is a secondary complication of many conditions, including asthma, congenital heart disease, chronic obstructive pulmonary disease, bronchiolitis obliterans (chronic rejection), pulmonary fibrosis, thrombosis, high blood pressure, autoimmune diseases, connective tissue diseases, human immunodeficiency virus, and cancer.[15] Lungs from individuals inflicted with PHT are unsuitable for transplantation[3]; however, decellularization of these organs may provide an acellular scaffold appropriate for recellularization with healthy autologous cells.

Monocrotaline (MCT)-induced PHT (MCT-PHT) is a well-established model of this disease in rats.[18,19] MCT is a toxic pyrrolizidine alkaloid derived from the rattlepod plant *Crotalaria spectabilis*. MCT is metabolized by the liver into a biologically active toxin that is carried by red blood cells to the lung leading to pulmonary vascular hypertrophy, intimal fibrosis, endothelial cell damage, pulmonary vasculitis, PHT, and right ventricular hypertrophy.[20–25] These manifestations closely resemble the clinical presentation of PHT in humans; therefore, MCT is an appropriate model to study the regeneration of PHT-diseased lungs using decellularization and recellularization.

The use of stem cells in regenerative medicine has generated a great deal of interest due to their ease of isolation from multiple sources, including embryonic and adult tissues, as well as their ability to differentiate into diverse cell lineages.[26–29] Both embryonic stem cells (ESCs) and mesenchymal stem cells (MSCs) from umbilical cord blood and adult bone marrow have been shown to differentiate into respiratory epithelial cells *in vitro*.[30–35] Stem cells are being avidly explored as a means to regenerate or repair functional pulmonary tissues for the treatment of lung injury and disease.[36–41] Bioartificial tissue regeneration relies on the interaction of these cells with the ECM proteins of decellularized organ scaffolds. Recent studies have shown that the ECM contributes to the functional behavior of MSCs and may be essential in guiding cell fate during tissue-specific differentiation.[42–47] Our group has recently demonstrated that bone marrow- and adipose-derived MSCs adhere to and proliferate within decellularized lung scaffolds in a rhesus macaque model of lung tissue engineering.[13] Here, the initial interaction of adipose-derived MSCs with decellularized scaffolds generated from MCT-PHT rat lungs is described in an effort to provide the necessary proof-of-principle that bioartificial organs can be derived from diseased sources.

Methods

Monocrotaline-induced pulmonary hypertension

All studies were approved by the Institutional Animal Care and Use Committee at Tulane University. A 25 mg/mL solution of MCT (Sigma-Aldrich, St. Louis, MO) was prepared by dissolving in 1 N HCl, adjusting the pH to 7.4 using NaOH, and diluting with phosphate-buffered saline (PBS).[48] To induce PHT, male Sprague-Dawley rats, weighing between 250 and 300 g (Charles River Laboratories, Portage, MI), were anesthetized using isoflurane balanced with O_2 (maintained at 1 barr) and injected with 60 mg/kg MCT intraperitoneally (IP). Control animals were sham-injected with PBS (pH of 7.4) at a volume equivalent to that which was used for MCT injections. Rats were killed 4 weeks after the injection (Supplementary Fig. S1A; Supplementary Data are available online at www.liebertpub.com/tea).

Extraction of intact heart/lung blocs

Control and MCT-PHT rats were anesthetized with ketamine/xyalzine (80–110/5–10 mg/kg intramuscularly/intraperitoneally) and supinated. The animals were then injected with 1 mL of PBS containing heparin (300 U/kg) for anticoagulation and sodium nitroprusside (SNP; 5 μg/kg) for vasodilation via the jugular vein. A laparotomy was performed 10 min after infusion of the heparin-SNP solution. Abdominal organs were carefully moved to reveal the distal abdominal vena cava. The animals were killed and exsanguinated by laceration of the abdominal vena cava while ~20 mL of the heparin-SNP saline solution was injected (~10 mL/min) into the pulmonary artery by the way of the right ventricle to perfuse the lungs *in situ*. Following exsanguination and perfusion, the heart and lungs were removed en bloc by

transecting the trachea proximal to the larynx and dissecting the dorsal connective tissues, esophagus, aorta, and vena cava.

Whole-lung decellularization

Lungs were decellularized by slight modifications to a protocol originally described by Price *et al.*[9] Briefly, the trachea and the pulmonary artery were cannulated and the left atrium was lacerated to allow decellularization solutions to easily drain from the vasculature. The pulmonary vasculature was perfused via the pulmonary artery cannula using a gravity-driven apparatus in which a column of liquid (10-mL syringe; BD Biosciences, San Jose, CA) was suspended 22 cm above the lung (Supplementary Fig. S1B). The lungs were perfused with ~10 mL of deionized water (DI water) instilled via the aforementioned gravity-driven apparatus. Then, the lungs were instilled with 10 mL of DI water by intratracheal inflation with a 10-mL syringe (Supplementary Fig. S1C). The DI water was allowed to drain from the lung by natural recoil. Perfusion followed by intratracheal instillation of DI water was repeated four more times. As depicted in Supplementary Figure S1D, 0.1% Triton X-100 (Sigma-Aldrich) was delivered to the lungs and pulmonary vasculature as before. The lungs were submerged in 0.1% Triton X-100 and incubated statically at 4°C overnight. The following day, the lungs were removed from the Triton solution and washed five times with DI water through the vasculature and the airway as before. The lungs were then inflated and perfused with 2% sodium deoxycholate (SDC; Fisher Scientific, Pittsburgh, PA) followed by an overnight incubation at 4°C. The next day, the lungs were removed from the SDC solution and washed five times with DI water as before. The lungs were then inflated and perfused with hypertonic saline (1 M NaCl) and incubated in this solution for 1 h at room temperature. After incubation in hypertonic saline, the lungs were washed with DI water and then inflated and perfused with a solution of 30 μg/mL DNase (Sigma-Aldrich DN25), 1.3 mM $MgSO_4$, and 2 mM $CaCl_2$. The lungs were incubated in this solution for 1 h at room temperature followed by five washes with PBS (without Ca^{2+}/Mg^{2+}) containing 500 U/mL penicillin, 500 μg/mL streptomycin, and 1.25 μg/mL amphotericin B. Decellularized lungs were stored in this solution at 4°C until needed.

Inflation fixation

Native and decellularized lung tissues from control and MCT-PHT animals were preserved by inflation-fixation with 10% neutral-buffered formalin (NBF) delivered intratracheally by gravity at ~25 cm H_2O while the lungs were also bathed in NBF. A peristaltic pump circulated NBF from the bathing reservoir back up to a syringe maintained at ~25 cm above the tissue over a period of 45 min. Fixed lungs were stored in NBF before dissection and histological analysis. For other analyses, fresh native and decellularized lung tissues were flash-frozen in liquid nitrogen and then stored at −80°C until needed.

Histological characterization

Slices of lung tissue of ~0.5 cm thick were cut from inflation-fixed native or decellularized lung tissues, embedded in paraffin, cut into 5 μm sections, and mounted onto glass microscope slides. Sections were stained with hematoxylin and eosin (H&E), Gömöri trichrome, modified Movat's pentachrome, and Alcian blue histological stains by the Center for Stem Cell Research and Regenerative Medicine Histology Core Facility using standard protocols. Stained slides were scanned using the Aperio ScanScope (Aperio, Vista, CA) at an initial magnification of 40×. Images were then captured and analyzed using the Aperio ImageScope program.

Genomic DNA extraction and quantification

The Qiagen DNeasy kit (Valencia, CA) was used to isolate genomic DNA (gDNA) from native and decellularized lungs. Briefly, blot-dried lung tissue was cut into small pieces and minced. Minced tissues were weighed and combined to total 25 mg per sample. Each sample was processed identically according to the manufacturer's instructions. gDNA was quantified using a NanoDrop 2000c spectrophotometer (Thermo-Fisher Scientific, Waltham, MA). Two-way analysis of variance (ANOVA) was used to compare control native, MCT native, control decellularized, and MCT decellularized lung gDNA yield per 25 mg tissue.

To facilitate equal loading for DNA gel electrophoresis, gDNA isolated from decellularized lungs was precipitated by adding 0.1 volumes of 3 M sodium acetate followed by 2.5 volumes of 100% ethanol. Precipitated DNA was pelleted by centrifugation at 14,000 rpm for 10 min. The pellet was washed with 70% ethanol and centrifuged again at 14,000 rpm for 10 min. The supernatant was removed, and the pellets were allowed to air dry for an hour before dissolving in nuclease-free water.

Five hundred nanograms of gDNA from control native, MCT native, control decellularized, and MCT decellularized lungs was loaded into a 0.8% Ultrapure agarose gel (Invitrogen, Carlsbad, CA) and separated by electrophoresis at 80 V for ~1 h. Gels were visualized by UV transillumination and imaged using the GE ImageQuant LAS 4000 system (GE Healthcare, Piscataway, NJ).

Western blot

Protein lysates from native and decellularized lungs were prepared as follows. Lung tissue was cut into small sections with scissors and then minced using a razor blade. Minced tissue was homogenized in a prechilled Dounce homogenizer containing RIPA buffer and 1× HALT protease inhibitor cocktail (Thermo-Fisher Scientific). The tissue was incubated for 30 min at 4°C with gentle rotation. The lysates were cleared by centrifugation at 14,000 *g* for 10 min at 4°C. The supernatants were collected and protein concentrations were determined using the BCA assay (Pierce, Rockford, IL). Protein lysates derived from decellularized lungs were concentrated by centrifuging at 4000 rpm for 5 min in Millipore (Billerica, MA) Ultracel-3K centrifugal filter devices. This step was necessary because lysates from decellularized lungs were dilute in protein concentration due to the lack of cell-associated soluble proteins.

Thirty micrograms of protein lysate was combined with NuPage LDS Sample Buffer and NuPage Reducing Agent (Invitrogen) according to the manufacturer's instructions. Samples were then boiled at 100°C for 5 min to denature the

protein. Samples were loaded into NuPage 4–12% gradient gels (Invitrogen) for electrophoresis at 200 V for 1 h. A 1:1 mixture of Magic Mark XP (Invitrogen) and Precision Plus Protein Kaleidoscope (Bio-Rad, Hercules, CA) was used as a molecular weight marker. The proteins were transferred from the gel to nitrocellulose membranes using the Invitrogen iBlot semi-dry transfer system. Membranes were stained with Ponceau S (Sigma-Aldrich) for 5 min and photographed to confirm equal protein loading by densitometry. To remove the Ponceau S stain, membranes were rinsed with DI water three times followed by a 15-min incubation in DI water. Membranes were then washed once for 5 min with PBS containing 0.1% Tween-20 (PBS-T) before blocking with PBS-T containing 5% reagent-grade blocking dry milk (Bio-Rad) and 1% goat serum. Membranes were blocked for 2 h at room temperature on a shaking platform. Membranes were then incubated overnight with gentle shaking at 4°C with blocking solution containing primary antibody (Supplementary Table S1). On the next day, membranes were washed 3 × 5 min with PBS-T and then incubated with gentle shaking for 1 h at room temperature in blocking solution containing 1:2000 goat anti-rabbit immunoglobulin G (IgG)–horseradish peroxidase (HRP) (Cell Signaling, Danvers, MA) or goat anti-mouse IgG-HRP (Santa Cruz Biotechnology, Santa Cruz, CA). Membranes were washed 2 × 5 min then once for 15 min in PBS-T. Membranes were incubated for 1 min with enhanced chemiluminescence reagent (Invitrogen) and visualized using the GE ImageQuant LAS 4000 system.

Immunohistochemistry

Immunohistochemistry (IHC) was performed on 5 μm lung sections of native and decellularized lung tissues using antibodies listed in Supplementary Table S1. Briefly, slides were deparaffinized by warming on a heating platform at 57°C for at least 30 min followed by incubation in the Histochoice solvent (Amresco, Solon, OH) and rehydration through ethanol to water. Depending on the recommendations from the antibody provider, antigen retrieval was performed either enzymatically by incubating the tissue sections with proteinase K (400 μg/mL in 20 mM Tris pH 8.0) for 15 min at 37°C in a humidified chamber or antigen retrieval was heat mediated by submerging the tissue sections in sub-boiling sodium citrate (10 mM, 0.05% Tween-20, pH 6.0) for 10 min. Slides were blocked with 10% normal serum (from the secondary antibody host animal) and 1% bovine serum albumin (BSA) in Tris-buffered saline (TBS) for 2 h at room temperature in a humidified chamber. The slides were then incubated with a primary antibody (diluted in TBS with 1% BSA) overnight at 4°C in a humidified chamber. Following incubation, slides were extensively washed with TBS-T (TBS containing 0.05% Tween-20). Slides were incubated with a secondary antibody (diluted 1:200 in TBS with 1% BSA) for 1 h at room temperature in a humidified chamber protected from light. The secondary antibody was either AlexaFluor 594 goat anti-rabbit IgG (H + L) or AlexaFluor 594 goat anti-mouse IgG (H + L) from Invitrogen. After incubation with a secondary antibody, slides were washed with DI water and coverslips were mounted with Prolong Gold Anti-fade Reagent with 4′,6-diamidino-2-phenylindole (DAPI) (Invitrogen). Isotype and secondary antibody-only controls were performed to distinguish nonspecific antibody binding (Supplementary Fig. S2). Images were captured using the Leica DMRXA2 deconvolution inverted fluorescent microscope (Leica Microsystems, Buffalo Grove, IL) fitted with the Cooke SensiCAM camera/controller and Slidebook software.

Proteomics

Whole native and decellularized lungs were dissected into individual lobes and snap-frozen in liquid nitrogen. Using a chilled mortar and pestle, the frozen tissue was ground into a powder and then incubated in RIPA buffer containing 1× HALT protease inhibitor cocktail for 30 min at 4°C with shaking. The lysates were then centrifuged at 14,000 *g* for 10 min at 4°C, and the supernatant was collected. The protein concentration of the supernatant was determined using a BCA assay. For collection of native protein lysate, one whole lung was used. For collection of decellularized lung protein lysate, three decellularized whole lung lysates were pooled and concentrated using Millipore Ultracel 3K centrifugal filters. Proteomic analyses were performed by the RCMI Core facilities at the Xavier University of Louisiana in New Orleans as previously described.[13] Briefly, 100 μg of each sample lysate was processed for analysis by high-performance liquid chromatography coupled with tandem mass spectrometry (LC-MS/MS). Protein samples were trypsin-digested, desalted, lyophilized, and then analyzed using an LTQ-Orbitrap XL (Thermo-Fisher Scientific) interfaced with an Ultimate 3000 Dionex nanoflow HPLC system (Dionex, Sunnyvale, CA). Peptides were identified using high mass resolution measurement of the parent ion and its product ions generated by collision-induced dissociation of a reporter ion. The Mascot (Matrix Science, Boston, MA) protein search algorithm was used for the database search. Proteome Discoverer 1.2 software (Thermo-Fisher Scientific) generated Mascot format files using the following criteria: database, IPI.Rat.fasta.v3.77; enzyme, trypsin; maximum missed cleavages, 2; static modifications, carbamidomethylation (+57 Da), N-terminal TMT6plex (+229 Da), lysyl TMT6plex (+229 Da); dynamic modifications, N-terminal Gln-pyro-Glu (−17 Da); methionine oxidation (+16 Da); STY phosphorylation (+80 Da); MS peptide tolerance set to 15 ppm; MS/MS tolerance set to 0.05 Da. Peptides identified by the search engine were accepted only if they met the false discovery rate of $p < 0.05$ (target decoy database). Identified peptides were sorted according to subcellular localization: cytoplasmic/intracellular, cytoskeletal, membrane, nuclear, mitochondrial, ECM (nonsecreted components), and secreted (non-ECM components). The percentage of peptides sorted to each category was determined. Because some peptides belong to multiple categories, the percentages total to greater than 100%.

Vascular casting of decellularized lungs

To confirm that the vasculature of decellularized lungs remains intact after decellularization, red Microfil liquid compound (Flow Tech, Inc., Carver, MA) was prepared at a ratio of 52.9% Microfil MV-130 Red, 42.3% MV dilutent, and 4.76% curing agent. This mixture was perfused through

the pulmonary arterial vasculature of native and decellularized lungs via the pulmonary artery cannula using a perfusion pump (Cole-Parmer, Vernon Hills, IL). Fourteen LS Masterflex tubing (Cole-Parmer) was used to instill Microfil into the vasculature at a rate of 1 mL/min for 5 min. Next, ~10 mL of 2% low melting point (LMP) agarose (Invitrogen) was injected into the airway while the vasculature was perfused with Microfil for an additional 5 min at 1 mL/min. This was followed by perfusion at a rate of 0.1 mL/min for 15 min to provide a constant pressure while the Microfil polymerized. While still connected to the perfusion pump, the lungs were statically incubated for 15 min to allow complete polymerization of the casting agent and solidification of the agarose. The casted agar-inflated lungs were submerged in 10% NBF and stored at 4°C.

Native and decellularized lung vascular casts were visualized using a vivaCT-40 (SCANCO Medical, Wayne, PA). MicroCT slices were obtained at 38 μm voxel size, 45 kV peak x-ray tube voltage, 88 μA tube current, and standard resolution (250 pictures per 180°). Integration time was 650 ms with continuous rotation. Scans took ~70–80 min and resulted in ~1100– 1300 serial sections through ~45 mm (longitudinally) of lung tissue. Data files were converted to DICOM (Digital Imaging and Communications in Medicine) format for analysis in ImageJ (version 1.47p). Images were imported into ImageJ as a sequence and analyzed using the BoneJ plugin (version 1.3.10) by adjusting the threshold to highlight the vascular cast in the foreground and converting the image sequence to binary mode. BoneJ's ''Thickness'' algorithm was used to determine the average diameter of the vascular casts and to generate a heatmap of the casts where larger diameter vessels are orange and smaller diameter vessels are purple (Supplementary Figure S3). The Thickness algorithm determines the thickness at a point as the diameter of the largest sphere that fits within the structure at that point. Only the foreground (vascular cast) of the binary image was analyzed. The heatmap graphic generated by the algorithm represents the thickness at each point within the structure. The heatmap of the vascular cast was visualized using the 3D Viewer application in ImageJ.

Airway seeding of acellular matrices with ASCs

Sprague-Dawley rat adipose-derived stem cells (rASCs) were graciously provided by Dr. Jeffrey Gimble at the Pennington Biomedical Research Center (Baton Rouge, LA). rASCs were cultured in complete culture media (CCM) comprising alpha-modified Eagle's medium containing 16.4% fetal calf serum, 4 mM L-glutamine, 100 U/mL penicillin, 100 μg/mL streptomycin, and 250 ng/mL amphotericin B at 37°C, 5% CO_2. Decellularized lungs were washed thrice with PBS containing 500 U/mL penicillin, 500 μg/mL streptomycin, and 1.25 μg/mL amphotericin B and then thrice with CCM warmed to 37°C. rASC cultures at ~70% confluence were lifted using 0.25% trypsin, pelleted by centrifuging at 1500 rpm for 7 min, and resuspended in CCM at a density of 1 million cells/mL. This suspension was combined with 2% LMP agarose (1:1) for a final concentration of 500,000 cells/mL in 1% LMP agarose. As shown in Supplementary Figure S4, 10 mL of the cell–media–agar mixture was then instilled into decellularized lungs through the trachea, and the seeded lungs were transferred to PBS in a 4°C bath for 30 min to solidify the agarose. The cell-seeded lungs were cut into 1 mm slices using a Krumdieck Tissue Slicer (Alabama Research and Development, Munford, AL). Tissue slices were cultured with 2 mL of CCM in a six-well tissue culture dish. The media were changed every other day, and the slices were flipped daily to evenly distribute nutrients and oxygen to the cells dispersed throughout the tissue slices. Slices were collected 24 h, 3 days, 7 days, and 14 days after culture to assess the attachment and survival of the instilled rASCs. Slices were washed with PBS and fixed in 10% NBF before paraffin embedding, sectioning, and mounting onto glass slides for staining with H&E or for use in IHC analyses.

Vascular seeding of acellular matrices with ASCs

For vascular seeding, 8 mL of cell suspension (containing 1 million cells/mL in 1% LMP agarose) were perfused through the pulmonary vasculature. Ten milliliters of 2% LMP agarose was then instilled into the airway and allowed to solidify before 1-mm slices were cut using the Krumdieck Tissue Slicer. The media was changed every other day, and the slices were flipped daily. Slices were collected 24 hours, 3 days, 7 days, and 14 days after initial seeding and fixed in 10% NBF before histological processing.

Ki-67 staining for the determination of proliferation of seeded cells

Control and MCT-PHT scaffolds seeded with rASCs in either the vasculature or the airspace were stained with Ki-67 at various time points to determine the persistence of cells throughout slice culture. Tissue sections were deparaffinized and rehydrated as previously described in the IHC methods. Antigen retrieval was accomplished by incubating the tissue sections with proteinase K (400 μg/mL in 20 mM Tris pH 8.0) for 15 min at 37°C in a humidified chamber. Sections were blocked with TBS containing 10% goat serum and 1% BSA for 2 h at room temperature in a humidified chamber. Sections were stained with an anti-Ki-67 antibody (Abcam, Cambridge, MA) diluted 1:200 in TBS with 1% BSA overnight at 4°C in a humidified chamber. The following day, the tissue sections were incubated for 1 h at room temperature in a humidified chamber protected from light with AlexaFluor 594 goat anti-rabbit secondary antibody diluted 1:200 in TBS with 1% BSA. Ten random pictures were taken at 10× magnification using the Leica DMRXA2 deconvolution inverted fluorescent microscope fitted with a Cooke SensiCAM camera/controller and Slidebook software. For each picture, the total number of DAPI-stained cells and the number of Ki-67-stained cells were counted. The counts from all 10 pictures taken per sample were summed, and the total number of positively stained cells was divided by the total number of cells per field to determine the overall percentage of proliferating cells. Each time point was analyzed in triplicate.

Terminal deoxynucleotidyl transferase dUTP nick end labeling staining for the determination of apoptosis of seeded cells

Control and MCT-PHT scaffolds seeded with rASCs in either the vasculature or the airspace were stained for

terminal deoxynucleotidyl transferase dUTP nick end labeling (TUNEL), which is indicative of apoptosis. The *In Situ* Cell Death Detection Kit with Fluorescein from Roche (Indianapolis, IN) was used according to the manufacturer's instructions. Briefly, tissue sections were deparaffinized, rehydrated, and incubated with proteinase K (400 μg/mL in 20 mM Tris, pH 8.0) for 15 min at 37°C in a humidified chamber followed by staining with the TUNEL label and enzyme solutions. Negative controls were incubated with the label solution without enzyme. Positive controls were treated with 1000 U/mL DNase for 30 min at 37°C in a humidified chamber before TUNEL staining. Coverslips were mounted with the Prolong Gold Anti-fade Reagent containing DAPI (Invitrogen). Ten random pictures were taken at 10× magnification using the Leica deconvolution microscope. For each picture, the total number of DAPI-stained cells and the number of TUNEL-stained cells were counted. The counts from all 10 pictures taken per sample were summed, and the total number of positively stained cells was divided by the total number of cells per field to determine the overall percentage of cells undergoing apoptosis. Each time point was analyzed in triplicate.

Cell count determination

The average number of cells per field in rASC-seeded rat lung matrices from various time points was determined. For each sample, 10 random photos were taken at 5× magnification of the DAPI-stained tissue. The number of cells was counted, and the average number of cells per field was determined. Each time point was analyzed in triplicate.

Statistical analyses

gDNA quantification, Ki-67 staining, TUNEL staining, and cell count data were analyzed for statistical significance using a two-way ANOVA with Tukey's *post hoc* test between the groups. For DNA quantification, the two variables, which warranted the use of two-way ANOVA, were decellularization and disease. For Ki-67 staining, TUNEL staining, and cell count data, the two variables were disease and time. In addition to two-way ANOVA, one-way ANOVA was conducted for each scaffold and seeding location (i.e., control airway-seeded, MCT-PHT airway-seeded, control vascular-seeded, and MCT-PHT vascular-seeded) to determine whether time alone significantly affected the results. p-Values of < 0.05 were considered to be statistically significant.

Results

Detergents, salts, and enzymes effectively remove cells from rat lungs with MCT-PHT while retaining ECM structural components

Lungs from control rats and rats with MCT-PHT (Fig. 1A, B, respectively) were decellularized (Fig. 1C, D, respectively) using serial incubations in Triton X-100, SDC, hypertonic saline, and DNase. Characteristic of PHT, H&E staining of native lung tissue from MCT-PHT rats, depicted cell infiltration due to inflammation as well as hypertrophy and hyperplasia of cells surrounding blood vessels (Fig. 1B). Decellularization of control and MCT-PHT lungs efficiently removed cells as indicated by a lack of darkly stained nuclei and cellular material in tissue sections stained with H&E (Fig. 1C, D, respectively). The eosin-stained lung ECM ultrastructure of both control and MCT-PHT lungs remained intact after decellularization as indicated by the maintenance of alveolar (A), bronchiolar (B), and vascular (V) structures (Fig. 1C, D). Control and MCT-PHT lungs were also stained with Alcian Blue for glycosaminoglycans (GAGs), Gömöri trichrome for collagens, and Movat's modified pentachrome for elastins. Alcian Blue-stained GAGs were seen throughout native control and native MCT-PHT lungs and were well retained after decellularization. Collagen bundles stained green by Gömöri trichrome were seen around blood vessels and bronchioles as well as throughout the alveolar parenchyma in native control and native MCT-PHT rat lungs. The collagen stain was notably pronounced in native MCT-PHT lungs around hyperplastic blood vessels. In decellularized control and MCT-PHT lungs, Gomorï-stained collagen was prevalent throughout alveolar septae and more heavily around bronchial and vascular structures. Elastin fibers darkly stained by Movat's modified pentachrome were abundant throughout native control and native MCT-PHT lungs. Elastin staining was especially prevalent surrounding blood vessels and bronchioles. In native MCT-PHT lungs, heavy staining concentrated around hyperplastic blood vessels was observed. Elastin was maintained throughout alveolar septae (gray arrows), at the axes of respiratory bronchioles (black arrows), and surrounding bronchi and blood vessels in decellularized control and decellularized MCT-PHT lungs (Fig. 1C, D). Overall, staining revealed that decellularization removed cells from MCT-PHT rat lungs while retaining ECM ultrastructure and maintaining the molecular components of GAGs, collagens, and elastin similar to decellularized control lungs.

DNA is effectively removed by decellularization of MCT-PHT lungs

To further assess the efficiency of decellularization, gDNA was isolated from representative samples of native and decellularized control and MCT-PHT lungs and quantified (Fig. 2A). No significant difference between the DNA yield of control native lungs and MCT-PHT native lungs ($p = 0.4330$) was found. After decellularization, DNA was greatly reduced in both control decellularized and MCT-PHT decellularized lungs. DNA reduction was $\sim$30-fold in decellularized MCT-PHT lungs and 50-fold in decellularized control lungs. gDNA extracted from decellularized control lungs was significantly less ($p = 0.0009$) than that extracted from native control lungs. Similarly, gDNA extracted from decellularized MCT-PHT lungs was significantly less ($p = 0.0006$) than that extracted from native MCT-PHT lungs. There was no significant difference between the amounts of DNA recovered from decellularized control lungs and decellularized MCT-PHT lungs ($p = 0.9997$). Gel electrophoresis of 500 ng of DNA recovered from native control and native MCT-PHT lungs produced a heavy band of high-molecular-weight gDNA, whereas DNA recovered from decellularized control and decellularized MCT-PHT lungs produced low-molecular-weight smears, signifying that the bulk of the DNA was degraded and removed following the DNase treatment (Fig. 2B).

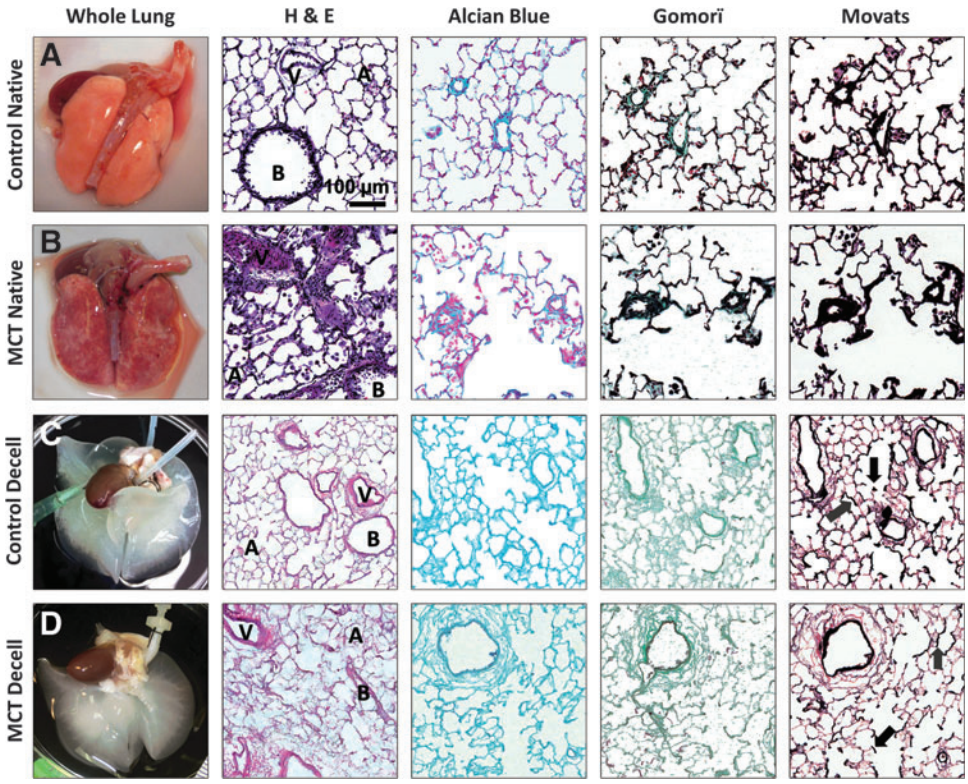

FIG. 1. Lungs from rats with monocrotaline-induced pulmonary hypertension (MCT-PHT) are decellularized similarly to normal control rat lungs and retain lung extracellular matrix (ECM) components. **(A)** Sham-injected control rat lungs were extracted and inflation fixed for histological analysis by hematoxylin and eosin (H&E) staining (dark purple nuclei and light pink ECM), Alcian Blue staining of glycosaminoglycans (GAGs, blue), Gömöri trichrome staining of collagen fibers (green), and Movat's Modified Pentachrome staining of elastin fibers (black). Pulmonary structures such as bronchi (B), blood vessels (V), and alveoli (A) were easily identifiable. **(B)** MCT-PHT rat lungs were similarly extracted, inflation fixed, and stained and showed hyperplasia of the cells of vascular walls, a feature that is characteristic of PHT. **(C)** Control rat lungs were decellularized using Triton X-100, sodium deoxycholate, hypertonic saline, and a DNase solutions. H&E staining revealed the removal of darkly staining nuclei with retention of alveolar, bronchial, and vascular structures. Alcian Blue, Gömöri, and Movat's staining indicated the retention of key ECM components, including elastin in alveolar septae (gray arrows) and at the axes of respiratory bronchioles (black arrows). **(D)** MCT-PHT rat lungs were decellularized, fixed, and stained as above. H&E staining showed efficient removal of cells despite PHT-associated hyperplasia. Alcian Blue, Gömöri, and Movat's staining showed retention of collagens, elastin, and GAGs, respectively, similar to decellularized control lungs. Color images available online at www.liebertpub.com/tea

ECM components are retained and enriched after decellularization of MCT-PHT lungs

Protein lysate from native and decellularized lungs was subjected to sodium dodecyl sulfate (SDS)–polyacrylamide gel electrophoresis and blotting for smooth muscle alpha actin (SMA), fibronectin, laminin, and GAPDH. Western blotting (Fig. 2C) showed that SMA was detectable in MCT-PHT lungs but not in control lungs after decellularization. Western blotting indicated that both fibronectin and laminin were enriched by decellularization in control and MCT-PHT lungs. Blotting for cellular protein GAPDH showed that cellular materials were adequately removed by decellularization as noted by the absence of detectable GAPDH in decellularized samples.

IHC staining for collagen I, collagen IV, collagen VI, elastin, laminin, SMA, and vitronectin was conducted to investigate the effect of decellularization on individual ECM components (Fig. 3). Basement membrane components collagen IV (Fig. 3E–H) and laminin (Fig. 3M–P) were retained in control and MCT-PHT lungs after decellularization. Collagen I stained bronchial and vascular structures heavily before and after decellularization of both control and MCT-PHT lungs (Fig. 3A–D). Collagen VI stained intensely throughout native and decellularized control and MCT-PHT lungs (Fig. 3I–L). Elastin stained most intensely around bronchial and vascular structures but only lightly throughout the parenchyma of decellularized control and decellularized MCT-PHT lungs (Fig. 3S, T, respectively). SMA appeared to stain more abundantly in native MCT-PHT lungs (Fig. 3V) than in native control lungs (Fig. 3U). After decellularization, SMA appeared to be depleted in control lungs (Fig. 3W) but was retained in MCT-PHT lungs (Fig. 3X), supporting a similar observation using Western blotting. Vitronectin stained lightly throughout native and decellularized lungs (Fig. 3Y, BB). Lack of DAPI staining in decellularized tissues validated that cells were efficiently removed by decellularization (insets). Ultimately, most ECM components were well preserved after decellularization of both control and MCT-PHT lungs.

Proteomic analysis of 100 µg of protein from one representative native lung or three pooled decellularized lungs

was conducted. Over 4000 peptides were identified in 100 μg of native lung samples, whereas approximately only 2000 were identified in 100 μg of pooled decellularized samples. ECM components accounted for < 1% of the total peptides identified in native control and native MCT-PHT lungs (Fig. 4). In comparison to native control lungs, native MCT-PHT lung lysate contained more peptides related to the blood/endothelium, including complement components, clotting factors, and globulins (14.99% vs. 6.68%; data not shown). After decellularization, ECM components comprised the largest constituent of identified peptides in decellularized lungs accounting for 31.6% of decellularized control lung peptides and 36.2% of decellularized MCT-PHT lung peptides (Fig. 4) signifying that decellularization enriches for ECM proteins (> 60-fold) while depleting cellular proteins.

Table 1 displays the top 10 most frequently identified peptides in native and decellularized lung protein lysates. Peptides identified as ECM components are listed in italics. No ECM protein-associated peptides were detected frequently enough in native lung samples to be ranked in the top 10. The highest ranked ECM protein-associated peptide was ranked 513 in native control lung lysate and 248 in native MCT-PHT lung lysate (data not shown). After decellularization, however, multiple ECM protein-associated peptides were ranked in the top 10 of decellularized control and decellularized MCT-PHT lungs with procollagen type 6 being the most frequently identified peptide in both the groups. More proteins related to smooth muscle, particularly myosin, were identified in decellularized MCT-PHT lungs than in decellularized control lungs (12.06% vs. 9.94%; data not shown) (Table 1).

The vascular network of hypertensive lungs is intact after decellularization

To determine whether the vascular compartment of decellularized lung scaffolds remains intact after detergent-mediated decellularization, the vasculature of representative decellularized control and decellularized MCT-PHT lungs were instilled with Microfil casting solution through the pulmonary artery using a perfusion pump. Native control and native MCT-PHT lungs were also casted for comparison. Vascular casts were visualized by microCT (Supplementary Fig. S3). MicroCT scans of the vascular casts from native and decellularized MCT-PHT lungs analyzed for vessel thickness depicted narrowed blood vessels characteristic of PHT. The average diameter of the vascular casts was estimated. The representative native MCT-PHT vascular cast had a mean vessel diameter of 0.109 ± 0.053 mm. The representative native control lungs had a mean vessel diameter of 0.128 ± 0.075 mm. The mean vessel diameter of

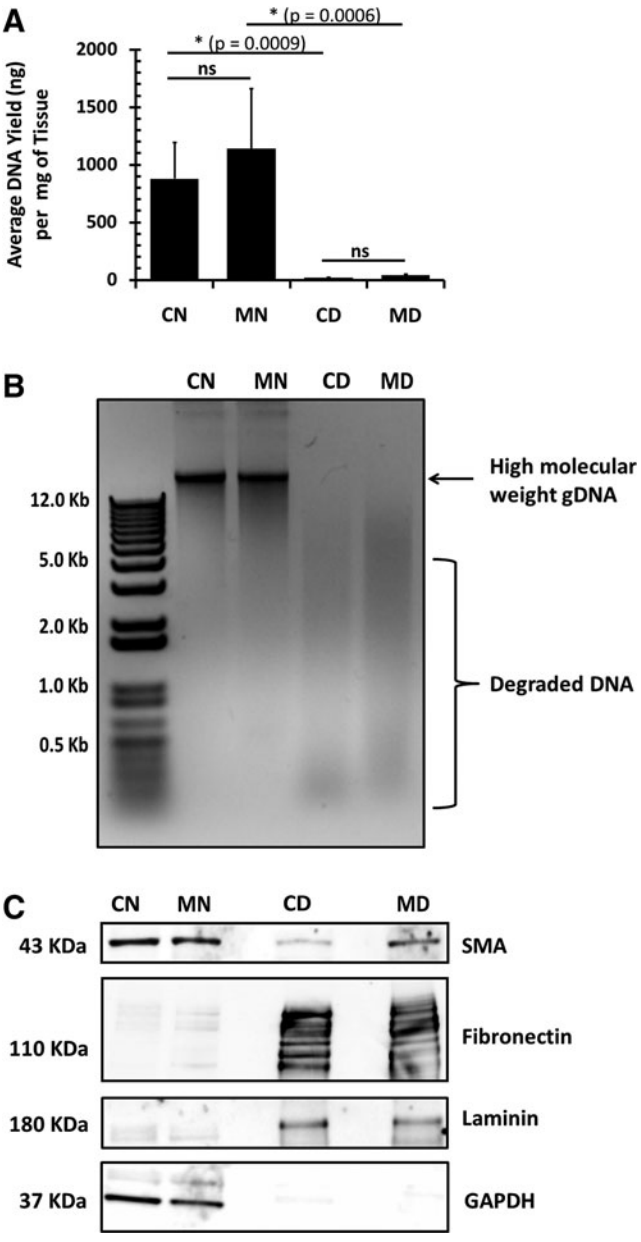

FIG. 2. Decellularization of MCT-PHT lungs depletes DNA and cellular components while enriching ECM proteins. **(A)** Genomic DNA (gDNA) was extracted from control native (CN), MCT-PHT native (MN), control decellularized (CD), and MCT-PHT decellularized (MD) lungs. Total gDNA extracted from decellularized lung tissues was significantly less than that from native lungs ($p < 0.001$). There was no significant difference between the amount of gDNA recovered from native control and native MCT-PHT lungs ($p > 0.05$; $n = 8$ for CN, $n = 9$ for MN). There was also no significant difference between the amount of DNA extracted from decellularized control and decellularized MCT-PHT lungs ($p > 0.05$; $n = 6$ for CD, $n = 3$ for MD). On average, decellularized control lungs contained 18.0 ng of DNA per milligram of tissue, whereas decellularized MCT-PHT lungs contained an average of 41.6 ng of DNA per milligram of tissue. **(B)** Gel electrophoresis of 500 ng of DNA isolated from each of the four samples indicated that the DNA extracted from decellularized lungs was highly degraded forming a smear rather than a distinct band. **(C)** Western blotting of smooth muscle actin (SMA), fibronectin, and laminin revealed that decellularization enriches ECM components while depleting cellular components such as glyceraldehyde 3-phosphate dehydrogenase (GAPDH). Decellularized MCT-PHT lung protein lysate produced a darker band for SMA than decellularized control lung lysate. Asterisks indicate $p < 0.001$ by two-way analysis of variance with Tukey's *post hoc* test. NS (not significant) indicates $p > 0.05$.

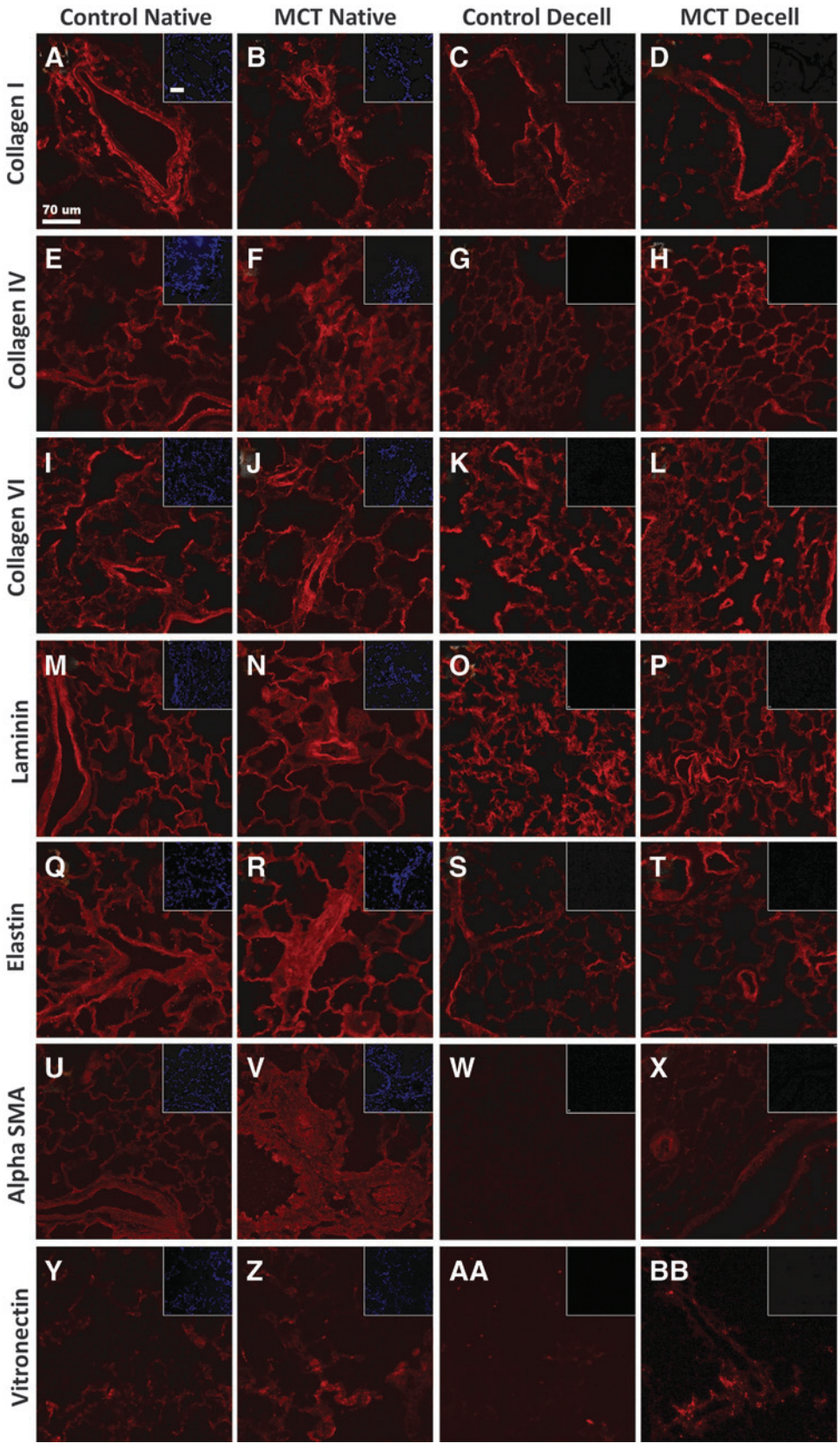

FIG. 3. Structural ECM components are retained in MCT-PHT lungs after decellularization. Native control lungs widely expressed collagen I **(A)**, collagen IV **(E)**, collagen VI **(I)**, and laminin **(M)**. Elastin **(Q)** and SMA **(U)** were detected in bronchi and large blood vessels but were only faintly detected throughout the lung parenchyma. Vitronectin **(Y)** was only marginally detected. Native MCT-PHT lungs similarly expressed these ECM components with some notable differences. Increased expression of collagen I **(B)**, collagen IV **(F)**, collagen VI **(J)**, laminin **(N)**, elastin **(R)**, SMA **(V)**, and vitronectin **(Z)** was seen around hyperplastic blood vessels. Decellularized control lungs retained collagen I **(C)**, collagen IV **(G)**, collagen VI **(K)**, laminin **(O)**, elastin **(S)**, and vitronectin **(AA)** but lost SMA **(W)**. Decellularized MCT-PHT lungs retained collagen I **(D)**, collagen IV **(H)**, collagen VI **(L)**, laminin **(P)**, elastin **(T)**, SMA **(X)**, and vitronectin **(BB).** Scale bars represent 70 μm. Color images available online at www.liebertpub.com/tea

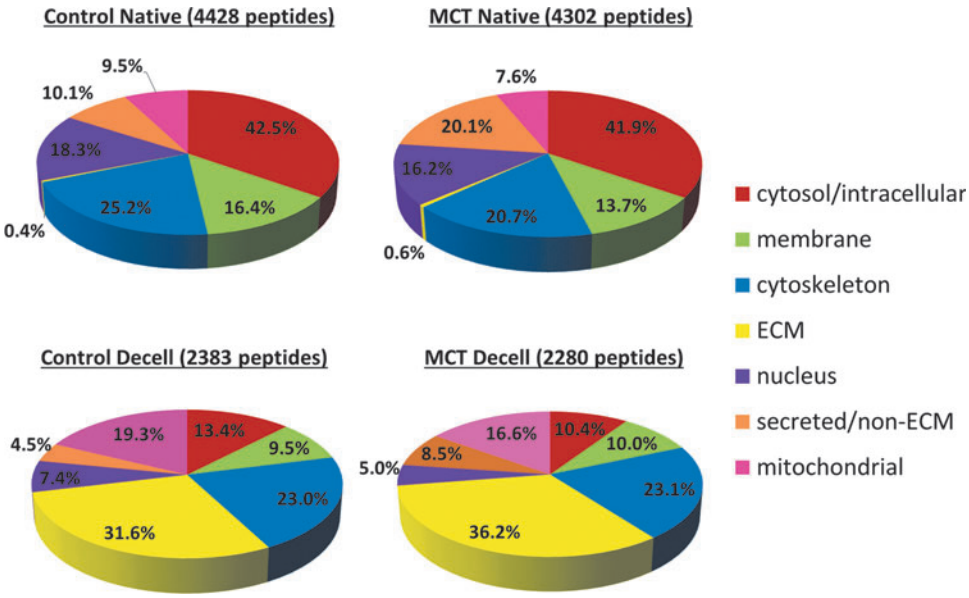

FIG. 4. ECM components comprise the majority of proteins extracted from decellularized MCT-PHT lungs. Over 4000 peptides were identified in 100 μg of protein extracted from native lungs, whereas only ~2000 peptides were identified in an equal amount of protein extracted from decellularized lungs. In both control and MCT-PHT native lungs, ECM proteins comprised less than 1% of the total peptides identified (0.4% of native control lungs and 0.6% of native MCT-PHT lungs). After decellularization, however, the majority of peptides in both the groups were ECM components (31.6% of decellularized control lungs and 36.2% of decellularized MCT-PHT lungs), although some subcellular components remained after decellularization. The total percentage exceeds 100% because some proteins were classified into multiple cellular and/or extracellular categories. For proteomics analysis, protein was extracted from one representative native lung or pooled from three decellularized lungs. Insets show DAPT staining. Color images available online at www.liebertpub.com/tea

the representative decellularized MCT-PHT vascular cast was 0.152 ± 0.134 mm. The representative control decellularized lung vascular cast had an average vessel diameter of 0.247 ± 0.160 mm. Overall, both the native and decellularized vascular casts of the MCT-PHT lungs had a smaller mean vessel diameter than their control counterpart. Decellularization appeared to lead to an increase in mean diameter seen in both the control and MCT-PHT scaffolds.

rASCs attach, survive, and proliferate in the airway and vascular compartments of hypertensive lung scaffolds

rASC-seeded and agar-inflated lungs were cut into 1-mm slices and cultured in CCM for 14 days. Lung slices were collected for analyses 24 h, 3 days, 7 days, and 14 days after the initial instillation of cells. H&E staining indicated that rASCs disbursed throughout control and MCT-PHT lung scaffolds and were maintained for up to 14 days (Fig. 5). When seeded into the airway, rASCs were seen lining bronchial lumens (Fig. 5C, G insets) and, in some areas, appear cuboidal (Fig. 5H inset) or columnar (Fig. 5C inset) in shape after 7 and 14 days in culture. When seeded into the vasculature, rASCs were retained in the vascular compartment and were not seen in the airspace at any time point. Additionally, rASCs appeared to attach and line the vascular walls (Fig. 5I–P). There did not appear to be any sign of hyperplasia or hypertrophy of rASCs seeded into the vasculature of any scaffold type at any time point.

To compare changes in cell density over time between control and MCT-PHT rASC-seeded lung slices, tissue sections were stained with DAPI to estimate cell number (Fig. 6A, B). The average number of cells per field was determined in triplicate for each time point (30 random fields total per sample). Control scaffolds seeded with rASCs in the airway contained ~26.23 ± 4.69 cells per field at 24 h (Fig. 6A). There was no significant difference between time points indicating that the starting cell number was maintained throughout the culture period ($p = 0.6514$). MCT-PHT scaffolds seeded with rASCs via the airway contained ~18.30 ± 3.40 cells per field at 24 h and maintained this number throughout the culture period ($p = 0.6647$). Although time did not significantly affect the number of cells per field, the source of the scaffold did ($p = 0.0003$). When seeded into the vasculature, ~6.33 ± 1.33 cells were seen per field in control scaffolds, and this number was maintained through the culture period (Fig. 6B; $p = 0.8122$). Approximately 4.13 ± 1.36 cells were seen in MCT-PHT scaffolds at 24 h, and this number was maintained throughout culture ($p = 0.7843$). Once again, the scaffold source, but not time, significantly affected the average number of cells per field of vascular-seeded scaffolds ($p = 0.0014$). Overall, the data demonstrate that rASCs attached and persisted in MCT-PHT scaffolds when seeded into either the airway or the vasculature, but in comparison with control scaffolds, MCT-PHT scaffolds accommodated the attachment and maintenance of fewer cells by our seeding and slice culture method.

To determine whether the rASCs instilled into the airway or vasculature of control and MCT-PHT scaffolds were proliferating, sections were stained for the cell proliferation marker Ki-67. At 24 h, 20.80 ± 2.74% of cells seeded into the airway of control scaffolds and 19.13 ± 4.89% of cells

Table 1. Top Ten Proteomics Database Search Results Ranked by Frequency of Peptides

Rank	Number of peptides	Description
Control native (CN)		
1	92	AHNAK nucleoprotein isoform 1
2	60	Talin-1
		Filamin, alpha
4	46	Serum albumin
5	32	Isoform 1 of Periaxin
6	30	Myosin-9
		Isoform 1 of serotransferrin
8	29	Clathrin heavy chain 1
9	27	Myosin-11
		Vinculin
		Nonerythroid spectrin beta
Monocrotaline native (MN)		
1	71	AHNAK nucleoprotein isoform 1
2	53	Talin-1
3	52	Filamin, alpha
4	51	Serum albumin
5	49	Complement C3 (Fragment)
6	41	Myosin-9
7	40	Alpha-1-macroglobulin
		Isoform 1 of murinoglobulin-1
9	37	Alpha-1-inhibitor 3
		Isoform 1 of Serotransferrin
Control decellularized (CD)		
1	79	*Procollagen, type VI, alpha 3*
		Procollagen, type VI, alpha 3 isoform
3	60	*Collagen type VI alpha 5-like*
		Perlecan
5	45	Filamin, alpha
		Myosin-6
7	39	*Fibronectin*
		Myosin, heavy chain 11, smooth muscle isoform 3
9	35	*Collagen, type VI, alpha 6*
10	31	*Laminin chain Fragment*
		Myosin-7
Monocrotaline decellularized (MD)		
1	81	*Procollagen, type VI, alpha 3*
2	79	*Procollagen, type VI, alpha 3 isoform*
3	65	*Collagen type VI alpha 5-like*
4	64	*Perlecan*
5	60	*Fibronectin*
6	56	Filamin, alpha
7	47	Myosin-9
8	43	Myosin-11
9	41	Myosin-6
10	37	Myosin-10
	37	*Laminin chain Fragment Lama5*

Proteins identified as ECM components are italicized.
ECM, extracellular matrix.

seeded into the airway of MCT-PHT scaffolds were proliferating (Fig. 6C). At 3 days and beyond, the number of cells proliferating dropped to about half the starting percentage. The scaffold source did not significantly influence the percentage of proliferating cells ($p = 0.8812$); however, time in culture did significantly affect the percentage of proliferating cells seeded in the airway ($p = 0.0002$). When seeded into the vasculature, similar percentages were seen with $17.26 \pm 6.30\%$ of cells in control scaffolds and $20.59 \pm 10.65\%$ of cells in MCT-PHT scaffolds initially proliferating at 24 h (Fig. 6D). This percentage dropped at day 3 and beyond in both control and MCT-PHT scaffolds. Neither scaffold source nor time significantly affected the percentage of proliferating cells seeded into the airway, although there was a trend indicating that time was a factor ($p = 0.0908$). Overall, the percentage of cells proliferating in MCT-PHT scaffolds was comparable to the percentage of cells proliferating in control scaffolds.

To analyze the extent of apoptosis occurring in the slice cultures, sections were subjected to TUNEL staining. At 24 h, $1.05 \pm 1.02\%$ of rASCs seeded into the airway of control scaffolds were TUNEL positive compared to $2.79 \pm 2.04\%$ of cells seeded into the airway of MCT-PHT lungs (Fig. 6E). There was no significant difference in the percentage of TUNEL-positive cells in the airway regardless of scaffold source or time point. When seeded into the vasculature, $2.66 \pm 0.10\%$ of rASCs in control scaffolds and $4.47 \pm 1.21\%$ of cells in MCT-PHT scaffolds were TUNEL positive (Fig. 6F). The scaffold source did not have a statistically significant effect on the apoptosis of cells in the vasculature, although the initial (24 h) percentage of apoptotic cells was higher in MCT-PHT scaffolds ($p = 0.0659$); however, time did significantly influence the percentage of apoptotic cells seeded into the vasculature ($p = 0.0013$). Overall, the percentage of apoptotic cells in MCT-PHT scaffolds was not statistically different than those in control scaffolds, although there was a trend in the vascular-seeded rASCs indicating a higher amount of apoptosis immediately after seeding.

The ECM components of MCT-PHT scaffolds are intact after seeding of rASCs in the airway or vasculature

To survey the ECM scaffolds after seeding of rASCs, seeded control and MCT-PHT scaffolds were collected, fixed, and stained for specific ECM proteins (Supplementary Fig. S5). Similar staining of the scaffolds shown previously (Fig. 3) was observed; however, colocalization of elastin staining with DAPI staining was seen in scaffolds seeded with rASCs in the airway or the vasculature (white arrows). Although staining for collagen I, collagen IV, collagen VI, and laminin was mainly seen throughout the matrix, occasionally, ECM staining colocalized with the DAPI-stained cells (white arrows) or stained brightly in the area surrounding the cells (gray arrows). Vitronectin staining was no longer detectable, whereas SMA staining was seen mainly near DAPI-stained cells but not throughout the matrix.

Discussion

The results of this study indicate that in a rat model of PHT, diseased lungs can be efficiently decellularized and can likewise be seeded with stem cells for lung regeneration strategies. Our data suggest that lungs deemed unsuitable for transplantation may have potential tissue engineering applications through decellularization. Decellularization technology is at the forefront of tissue engineering, but the

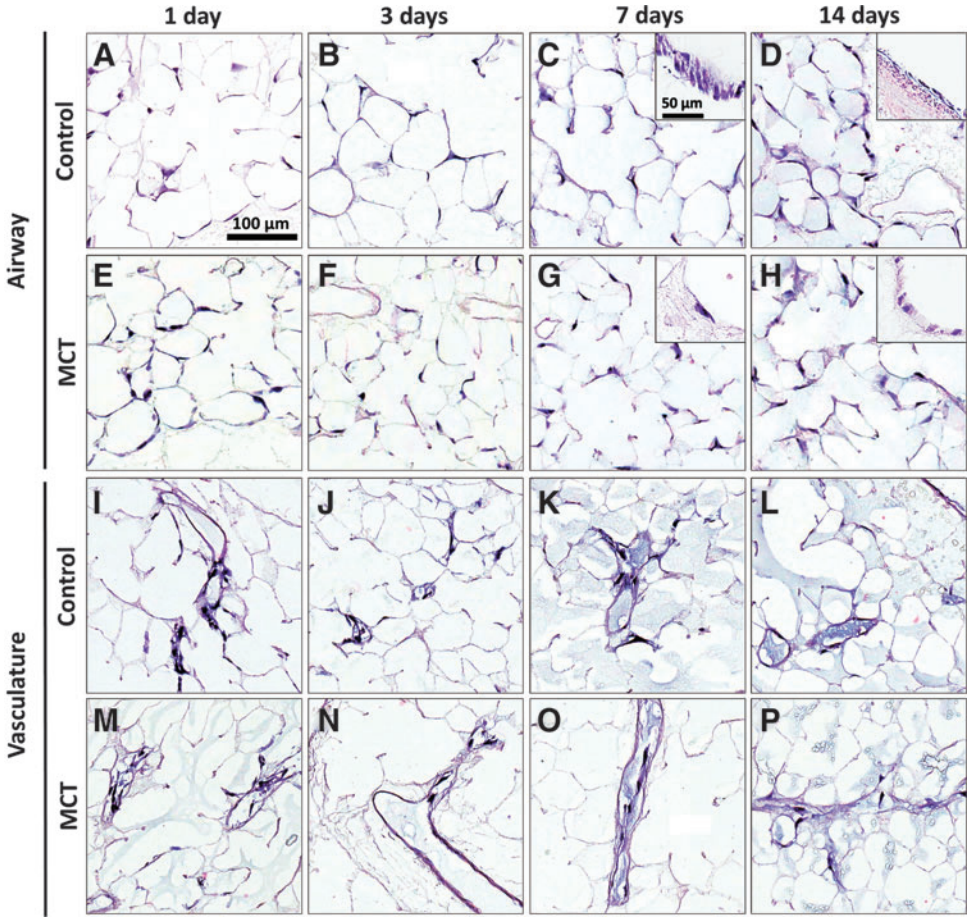

FIG. 5. Rat adipose-derived stem cells (ASCs) attach to and are maintained within MCT-PHT lung scaffolds in slice culture. Rat ASCs seeded into the airway of control **(A–D)** and MCT-PHT **(E–H)** scaffolds adhered to the airway ECM and persisted in slice culture. At 7 and 14 days, morphological changes were observed in cells attached to the ECM of bronchi in both control and MCT-PHT scaffolds (insets). **(I–P)** Rat ASCs seeded into the vasculature attached to the ECM of large blood vessels as well as capillaries but were not found in the airspace. No obvious morphological changes were observed in cells seeded into the vasculature after 14 days in culture. Scale bars indicate 100 µm in main images and 50 µm in inset images. Color images available online at www.liebertpub.com/tea

clinical feasibility, application, and implementation of this technology are not yet clear. In order for decellularization techniques to be clinically relevant, reengineered organs should be able to be derived from sources which are traditionally unsuitable for transplantation. According to the Organ Procurement and Transplantation Network's Annual Report for 2011, ~22.4% of lungs recovered for transplant were discarded due to poor organ function; 19.6% were discarded due to anatomical abnormalities; 9.3% of lungs were discarded because they were diseased, and 6.5% were discarded due to organ trauma; another 4% of lungs were discarded due to vascular damage, infection, or the warm ischemic time being too long.[49] If these discarded lungs could be made suitable for transplantation by decellularization-based tissue engineering, these organs would be able to decrease transplant wait times and potentially increase successful outcomes.

Previous work by Booth *et al.* and Sokocevic *et al.* suggested that decellularized lung tissue with extensive ECM remodeling, as is seen in fibrotic and emphysematous lung diseases, may not be ideal support structures for recellularization and eventual lung tissue engineering due to the obliteration of the structure of the alveoli.[50,51] Our work, however, utilized a disease model with pathology predominantly in the vasculature, the chief issue being hypertrophy and hyperplasia of the cells of the vascular wall. Unlike pulmonary fibrosis and chronic lower respiratory diseases such as emphysema and asthma, the ultrastructure of the airspace of the lung is not extensively remodeled by PHT.[52,53]

Decellularization effectively removed cells from MCT-PHT lungs, despite the vascular wall hyperplasia and hypertrophy associated with PHT. In addition, the ECM ultrastructure of the lung, including alveolar sacs, respiratory bronchioles, bronchi, and blood vessels, was maintained in MCT-PHT lungs after decellularization similar to decellularized control lungs. The maintenance of the 3D structure of the lung can potentially provide important mechanical cues that will aid in organized cell attachment and eventual recellularization of the lung scaffold.[54] In addition to structure, matrix composition will also be crucial to successful tissue engineering, particularly if progenitor cells are used as a cell source for recellularization. Matrix stiffness, governed mainly by the composition of collagen and elastin, has been shown to influence stem cell fate.[55] In this present study, collagen and elastin histological staining was seen in the parenchyma and surrounding bronchial and vascular structures of decellularized control and native MCT-PHT lung tissues. Axial and septal alveolar elastin was also observed by histological staining, but staining appeared lighter in the parenchyma of lungs after cells were removed. Some loss of ECM components would not be unexpected after treatment with detergents. Petersen *et al.* have shown that decellularization with either CHAPS detergent or SDS depleted 60% of elastin and 95% of GAGs; SDS depleted ~80% of collagen.[56] Price *et al.* noted that decellularization

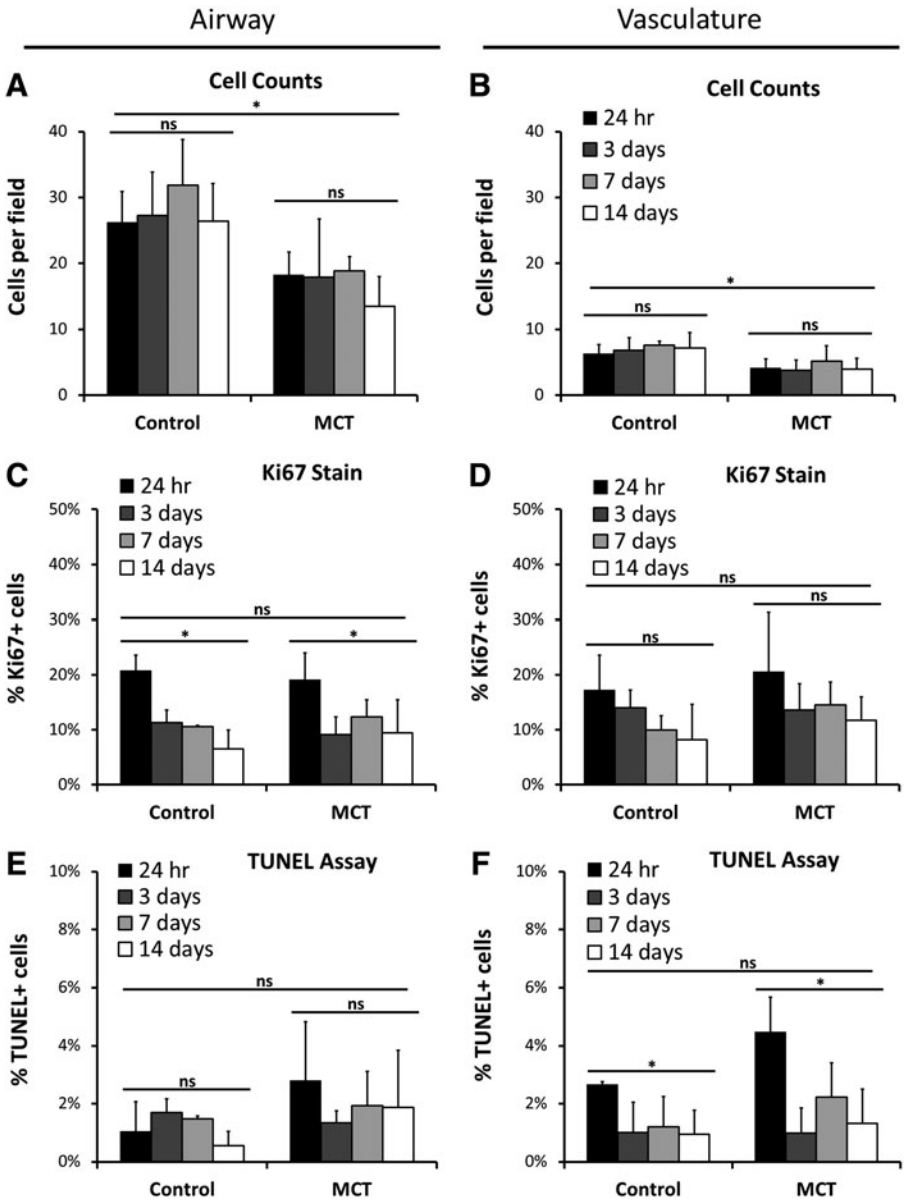

FIG. 6. Seeded cell number is maintained in slice cultures with similar prevalence of proliferation and apoptosis. The number of rat ASCs per field was determined by counting the number of 4′,6-diamidino-2-phenylindole-stained nuclei in 10 random images. MCT-PHT lung slices had significantly less seeded cells at 24 h in the airway **(A)** and vasculature **(B)** compared to control scaffolds ($p = 0.0003$ and $p = 0.0014$, respectively). However, the percentage of cells proliferating in the airway **(C)** or vasculature **(D)** of MCT-PHT scaffolds was comparable to control scaffolds ($p = 0.8812$ and $p = 0.2619$, respectively). Time in culture significantly reduced the percentage of proliferating cells in the airway ($p < 0.001$). The percentage of cell undergoing apoptosis in the airway **(E)** or vasculature **(F)** of MCT-PHT scaffolds was not significantly different from control scaffolds ($p = 0.1202$ and $p = 0.0659$, respectively). Time in culture significantly decreased the percentage of cells undergoing apoptosis in the vasculature ($p = 0.0013$). There was no significant interaction between time and scaffold source for cell count, Ki-67 staining, or TUNEL staining of cells seeded into the airway or vasculature. All analyses were conducted in triplicate. Asterisks indicate that $p < 0.01$ by two-way analysis of variance with Tukey's *post hoc* test. NS (not significant) indicates $p > 0.05$.

of mouse lungs using the detergents Triton X-100 and SDC maintained total collagen but reduced elastin, laminin, and GAG content.[9] Further work is needed to directly quantify these ECM components in MCT-PHT lung scaffolds.

Decellularized whole-organ matrices have the added clinical appeal of potentially being used to create patient-specific tissue by recellularization with autologous cells; therefore, it is important to minimize the potential immunogenicity of decellularized matrices by adequately removing cellular material and DNA. Here, decellularization was shown to significantly reduce the presence of gDNA in control and MCT-PHT lung scaffolds. Although not statistically significant, decellularized MCT-PHT lungs did contain slightly more DNA than decellularized control lungs. This translated to a ~30-fold reduction in DNA in MCT-PHT lungs compared to a ~50-fold reduction in control

lungs after decellularization. This could be due, in part, to the cell density around hypertrophic and hyperplastic vessels; the thickening of the vascular walls caused by PHT often leads to the occlusion of small arteries which, in turn, cuts off part of the lung from the blood supply.[52] During decellularization, occluded vessels could inhibit decellularization solutions from reaching the distal portions of the tissue. Previous studies also suggest that the difference in DNA content between normal and MCT-treated tissues may be due to smooth muscle hypertrophy associated with nuclear polyploidy.[57,58] When lysed from the cells, DNA can become difficult to remove from the matrix, especially if narrow blood vessels prevent efficient delivery of DNase to the tissue. The use of DNase in the decellularization procedure was able to degrade the DNA remaining in decellularized lungs after cells were lysed, as was indicated by gel electrophoresis; however, decellularized MCT-PHT lungs did contain some higher-molecular-weight DNA fragments. Whether this degraded DNA would be immunogenic must be addressed in subsequent work. It has been proposed by others that materials containing <50 ng of dsDNA per milligram (dry weight) ECM will not be immunogenic as long as the remaining DNA is degraded to <200 bp.[59–61] In fact, many commercially available biological scaffolds contain detectable amounts of DNA <200 bp, and these scaffolds have not been shown to cause adverse responses in the clinical setting.[61,62] In this study, decellularized MCT-PHT lung, on average, contained ~ 42 ng of gDNA per milligram of tissue; however, when electrophoresed, 500 ng of gDNA pooled from decellularized MCT-PHT lung samples contained fragments of DNA >200 bp. According to the aforementioned proposed standards for DNA removal from decellularized tissues, these data suggest that decellularized MCT-PHT lungs could be immunogenic. Quantification of the precise immune response to these decellularized scaffolds is warranted. In the future, increasing the concentration of DNase used during decellularization may facilitate further DNA degradation and removal from MCT-PHT lungs.

Due to the vascular pathology of PHT, it is feasible that MCT-PHT lung tissue could contain more vascular-associated proteins, particularly, SMA and myosin. Western blotting, IHC, and proteomics confirmed that decellularized MCT-PHT lungs retained more SMA and myosin than decellularized control lungs. It is unclear whether the remaining SMA and myosin will facilitate or hinder successful revascularization of the scaffold.

Western blotting also showed enrichment of fibronectin and laminin after decellularization. The banding pattern of fibronectin blotting presumably indicates that multiple isoforms of fibronectin were stained, although it is possible that fibronectin was degraded into uniform fractions. Because fibronectin is important to cell-ECM binding, further experimentation is necessary to determine if native fibronectin is intact after decellularization and how it will be involved in recellularization.

IHC, although not quantitative, illustrated the distribution of ECM components throughout decellularized matrices. Decellularization of MCT-PHT lungs produced ECM scaffolds that appeared to retain collagen I, collagen IV, collagen VI, laminin, and vitronectin comparable to decellularized control lungs. Elastin was retained in bronchial and vascular structures but appeared to be depleted from the parenchyma as was previously noted by Movat's staining. Loss of elastin may alter the stiffness and compliance of the matrix, which could, in turn, effect recellularization. Further investigation is needed to determine the full extent of elastin loss due to decellularization. Retention of the native distribution of the basement membrane components collagen IV and laminin will likely be valuable to recellularization. Although it cannot be concluded that these basement membrane proteins were not depleted or altered by decellularization, their IHC staining pattern appeared unchanged. Previous work by Cortiella *et al.* using freeze-thaw, detergent-decellularization revealed that both collagen IV and laminin were depleted from rat lungs; interestingly, when mouse ESCs were seeded into the matrices, they started to produce laminin and collagen IV.[12] It is possible that some matrix damage due to decellularization could induce seeded cells to remodel the matrix.[63] Recapitulating this natural response may be beneficial to recellularization. In the current study, staining of ECM proteins appeared to colocalize to rASCs seeded into MCT-PHT and control lung matrices. As noted by immunohistochemical staining, seeded rASCs appeared to produce elastin, a component that may have been depleted by decellularization. This supports the idea that these cells may secrete ECM proteins in their local environment for the purpose of creating the optimal cell attachment and proliferation surface.

Proteomic analysis confirmed on a larger scale what was observed by Western blotting for ECM components and GAPDH, that decellularization depleted cellular proteins and enriched ECM proteins. We were also able to survey the identified peptides to analyze the presence of proteins related to the endothelium and blood, which may be more prevalent in native MCT-PHT tissues due to hyperplasia, edema, and inflammation.[20,23,25] As predicted, a higher percentage of peptides categorized as blood/endothelial components was identified in native MCT-PHT lungs than in native control lungs. Surveying the top 10 most frequently identified peptides in each sample revealed that collagen VI was the most common peptide identified in decellularized lung tissues. To our knowledge, collagen VI has not been of particular interest to the field of lung decellularization. For the most part, the focus has been on collagen I and collagen IV due to their important contributions to structure. Daly *et al.* demonstrated the retention of collagen I and IV after decellularization of mouse lungs and subsequent recellularization with mouse bone marrow-derived stem cells (BMSCs).[11] Other groups, such as Price *et al.*, have surveyed collagen content by histological stains but have not specifically probed for collagen VI.[9] Collagen VI is a microfibrillar collagen known to associate with hyaluronan and believed to act as an anchoring element between structural collagen I/III and basement membrane proteins, such as collagen IV.[64,65] Thus, retention of collagen VI may aid in retention of collagens I, III, and IV. In the lungs, collagen VI is expressed in the bronchial and vascular walls and interstitial space, but increased expression of collagen VI by fibroblasts in early lung fibrosis has also been reported.[66,67] Collagen VI also serves as a cell binding substrate, which suggests that collagen VI may facilitate recellularization.[68] Investigation in other animal models of

decellularization will be helpful in determining the role that collagen VI will play in tissue engineering.

To investigate the ability of MCT-PHT lung scaffolds to support initial recellularization, scaffolds were seeded with rASCs. Our laboratory previously showed attachment and growth of rhesus macaque BMSCs and ASCs in acellular macaque lung scaffolds.[13] Daly *et al.* inoculated acellular mouse lungs with mouse BMSCs and showed that they persisted for 4 weeks in culture with some transient expression of the lung-specific thyroid transcription factor-1.[9,11] Cortiella *et al.* seeded acellular rat lungs with mouse ESCs and demonstrated that the cells expressed SMA, cytokeratin 18, and club cell (previously Clara cell) 10 protein (CC10) in a region-specific manner.[12] Taken together, these studies support the investigation of stem cells for recellularization of acellular lung scaffolds; however, there is a lack of data pertaining to the potential use of ASCs, especially in a disease model.

ASCs were used due to their ease of isolation from fat tissue, high yield, and clinical relevance, which make ASCs of particular interest to tissue engineering and regenerative applications, especially since ASCs are already being widely evaluated in clinical trials.[69,70] Though limited, there is some data to indicate that ASCs can differentiate into smooth muscle cells.[71] Thus, ASCs could be beneficial to investigating the application of lung scaffolds derived from a disease marked by smooth muscle pathology. In this present study, both MCT-PHT and control scaffolds supported the attachment and persistence of rASCs throughout the tissue slices for at least 14 days. Future studies will require the utilization of a more appropriate whole-organ culture and recellularization method involving a bioreactor system as has been successfully employed by other groups.[8–10]

Although the matrix composition and structure of MCT-PHT scaffolds appeared to be comparable to control scaffolds, the vascular lumenal volume was decreased. Whether this will negatively influence complete recellularization of MCT-PHT scaffolds and generation of healthy tissue is unclear. Theoretically, the narrowed vasculature may increase the shear stress and fluid stress experienced by cells seeded into the vasculature. Because shear stress and fluid stress have been linked to apoptosis and cell adherence as well as differentiation, additional work is needed to determine the precise effect of these stresses on cells seeded into MCT-PHT scaffolds.[72–78] If the effect impedes recellularization, MCT-PHT scaffolds may require additional manipulation, such as the introduction of matrix proteases, to increase lumenal diameter. On the other hand, recellularization may lead to turnover and remodeling of ECM deposits resulting from vascular remodeling in MCT-PHT. In the current study, colocalization of ECM staining and DAPI staining in seeded scaffolds suggested that recellularization contributed, in part, to ECM remodeling. Further examination of the applicability of lungs damaged by PHT to tissue engineering should focus on the influence of the MCT-PHT ECM scaffold on attachment, growth, and differentiation of seeded cells. Detailed investigation into the interaction of cells, particularly progenitor cells, with scaffolds derived from diseased tissues will provide insight into whether diseased scaffolds can be used to generate healthy tissue.

Conclusion

These studies confirm the possibility that decellularized lung scaffolds generated from diseased/damaged lungs may be suitable for tissue engineering strategies. Our data indicated that, similar to normal lung controls, lungs damaged by pulmonary hypertension can be decellularized with comparable efficiency, retain structural and molecular ECM components as to their normal counterparts, and can likewise be successfully seeded with stem cells for lung regeneration strategies.

Acknowledgments

The authors thank Dr. Edward Pankey and Dr. Philip Kadowitz of the Department of Pharmacology at the Tulane University School of Medicine for their assistance in acquiring MCT-PHT lung tissue. We thank Dr. Jeffery Gimble for supplying Sprague-Dawley rat adipose-derived stem cells. Finally, we also thank Dr. Ken Muneoka for granting us access to microCT imaging. Proteomic work was supported by the NIH grant 3G12MD007595-04.

Disclaimer

The content is the responsibility of the authors alone and does not necessarily reflect the views or policies of the Department of Health and Human Services nor does mention of trade names, commercial products, or organizations imply endorsement by the U.S. Government.

Disclosure Statement

No competing financial interests exist.

References

1. Organ Procurement and Transplantation Network (OPTN). http://optn.transplant.hrsa.gov (accessed Online 25 June 2013).
2. Van Raemdonck, D., Neyrinck, A., Verleden, G.M., Dupont, L., Coosemans, W., Decaluwe, H., Decker, G., De Leyn, P., Nafteux, P., and Lerut, T. Lung donor selection and management. Proc Am Thorac Soc **6,** 28, 2009.
3. Kotloff, R.M., and Thabut, G. Lung transplantation. Am J Respir Crit Care Med **184,** 159, 2011.
4. Ott, H.C., Matthiesen, T.S., Goh, S.K., Black, L.D., Kren, S.M., Netoff, T.I., and Taylor, D.A. Perfusion-decellularized matrix: using nature's platform to engineer a bioartificial heart. Nat Med **14,** 213, 2008.
5. Badylak, S.F., Taylor, D., and Uygun, K. Whole-organ tissue engineering: decellularization and recellularization of three-dimensional matrix scaffolds. Annu Rev Biomed Eng **13,** 27, 2011.
6. Song, J.J., Guyette, J.P., Gilpin, S.E., Gonzalez, G., Vacanti, J.P., and Ott, H.C. Regeneration and experimental orthotopic transplantation of a bioengineered kidney. Nat Med **19,** 646, 2013.
7. Barakat, O., Abbasi, S., Rodriguez, G., Rios, J., Wood, R.P., Ozaki, C., Holley, L.S., and Gauthier, P.K. Use of decellularized porcine liver for engineering humanized liver organ. J Surg Res **173,** e11, 2012.
8. Ott, H.C., Clippinger, B., Conrad, C., Schuetz, C., Pomerantseva, I., Ikonomou, L., Kotton, D., and Vacanti, J.P.

Regeneration and orthotopic transplantation of a bioartificial lung. Nat Med **16,** 927, 2010.
9. Price, A.P., England, K.A., Matson, A.M., Blazar, B.R., and Panoskaltsis-Mortari, A. Development of a decellularized lung bioreactor system for bioengineering the lung: the matrix reloaded. Tissue Eng Part A **16,** 2581, 2010.
10. Petersen, T.H., Calle, E.A., Zhao, L., Lee, E.J., Gui, L., Raredon, M.B., Gavrilov, K., Yi, T., Zhuang, Z.W., Breuer, C., Herzog, E., and Niklason, L.E. Tissue-engineered lungs for *in vivo* implantation. Science **329,** 538, 2010.
11. Daly, A.B., Wallis, J.M., Borg, Z.D., Bonvillain, R.W., Deng, B., Ballif, B.A., Jaworski, D.M., Allen, G.B., and Weiss, D.J. Initial binding and recellularization of decellularized mouse lung scaffolds with bone marrow-derived mesenchymal stromal cells. Tissue Eng Part A **18,** 1, 2012.
12. Cortiella, J., Niles, J., Cantu, A., Brettler, A., Pham, A., Vargas, G., Winston, S., Wang, J., Walls, S., and Nichols, J.E. Influence of acellular natural lung matrix on murine embryonic stem cell differentiation and tissue formation. Tissue Eng Part A **16,** 2565, 2010.
13. Bonvillain, R.W., Danchuk, S., Sullivan, D.E., Betancourt, A.M., Semon, J.A., Eagle, M.E., Mayeux, J.P., Gregory, A.N., Wang, G., Townley, I.K., Borg, Z.D., Weiss, D.J., and Bunnell, B.A. A nonhuman primate model of lung regeneration: detergent-mediated decellularization and initial *in vitro* recellularization with mesenchymal stem cells. Tissue Eng Part A **18,** 2437, 2012.
14. Song, J.J., Kim, S.S., Liu, Z., Madsen, J.C., Mathisen, D.J., Vacanti, J.P., and Ott, H.C. Enhanced *in vivo* function of bioartificial lungs in rats. Ann Thorac Surg **92,** 998, 2011.
15. McLaughlin, V.V., Archer, S.L., Badesch, D.B., Barst, R.J., Farber, H.W., Lindner, J.R., Mathier, M.A., McGoon, M.D., Park, M.H., Rosenson, R.S., Rubin, L.J., Tapson, V.F., Varga, J., American College of Cardiology Foundation Task Force on Expert Consensus Documents, American Heart Association, American College of Chest Physicians, American Thoracic Society, Inc, Pulmonary Hypertension Association. ACCF/AHA 2009 expert consensus document on pulmonary hypertension a report of the American College of Cardiology Foundation Task Force on Expert Consensus Documents and the American Heart Association developed in collaboration with the American College of Chest Physicians; American Thoracic Society, Inc.; and the Pulmonary Hypertension Association. J Am Coll Cardiol **53,** 1573, 2009.
16. Hassoun, P.M. Deciphering the ''matrix'' in pulmonary vascular remodelling. Eur Respir J **25,** 778, 2005.
17. O'Callaghan, D.S., Savale, L., Montani, D., Jais, X., Sitbon, O., Simonneau, G., and Humbert, M. Treatment of pulmonary arterial hypertension with targeted therapies. Nat Rev Cardiol **8,** 526, 2011.
18. Kay, J.M., and Heath, D. Observations on the pulmonary arteries and heart weight of rats fed on *Crotalaria spectabilis* seeds. J Pathol Bacteriol **92,** 385, 1966.
19. Kay, J.M., Harris, P., and Heath, D. Pulmonary hypertension produced in rats by ingestion of *Crotalaria spectabilis* seeds. Thorax **22,** 176, 1967.
20. Wilson, D.W., Segall, H.J., Pan, L.C., Lamé, M.W., Estep, J.E., and Morin, D. Mechanisms and pathology of monocrotaline pulmonary toxicity. Crit Rev Toxicol **22,** 307, 1992.
21. Heath, D., and Kay, J.M. Medical thickness of pulmonary trunk in rats with cor pulmonale induced by ingestion of *Crotalaria spectabilis* seeds. Cardiovasc Res **1,** 74, 1967.
22. Meyrick, B., and Reid, L. Development of pulmonary arterial changes in rats fed *Crotalaria spectabilis*. Am J Pathol **94,** 37, 1979.
23. Ghodsi, F., and Will, J.A. Changes in pulmonary structure and function induced by monocrotaline intoxication. Am J Physiol **240,** H149, 1981.
24. Gomez-Arroyo, J.G., Farkas, L., Alhussaini, A.A., Farkas, D., Kraskauskas, D., Voelkel, N.F., and Bogaard, H.J. The monocrotaline model of pulmonary hypertension in perspective. Am J Physiol Lung Cell Mol Physiol **302,** L363, 2012.
25. Rosenberg, H.C., and Rabinovitch, M. Endothelial injury and vascular reactivity in monocrotaline pulmonary hypertension. Am J Physiol **255,** H1484, 1988.
26. Kørbling, M., and Estrov, Z. Adult stem cells for tissue repair - a new therapeutic concept? N Engl J Med **349,** 570, 2003.
27. Longmire, T.A., Ikonomou, L., Hawkins, F., Christodoulou, C., Cao, Y., Jean, J.C., Kwok, L.W., Mou, H., Rajagopal, J., Shen, S.S., Dowton, A.A., Serra, M., Weiss, D.J., Green, M.D., Snoeck, H.W., Ramirez, M.I., and Kotton, D.N. Efficient derivation of purified lung and thyroid progenitors from embryonic stem cells. Cell Stem Cell **10,** 398, 2012.
28. Kadzik, R.S., and Morrisey, E.E. Directing lung endoderm differentiation in pluripotent stem cells. Cell Stem Cell **10,** 355, 2012.
29. Maroof, A.M., Keros, S., Tyson, J.A., Ying, S.W., Ganat, Y.M., Merkle, F.T., Liu, B., Goulburn, A., Stanley, E.G., Elefanty, A.G., Widmer, H.R., Eggan, K., Goldstein, P.A., Anderson, S.A., and Studer, L. Directed differentiation and functional maturation of cortical interneurons from human embryonic stem cells. Cell Stem Cell **12,** 559, 2013.
30. Rippon, H.J., Lane, S., Qin, M., Ismail, N.S., Wilson, M.R., Takata, M., and Bishop, A.E. Embryonic stem cells as a source of pulmonary epithelium *in vitro* and *in vivo*. Proc Am Thorac Soc **5,** 717, 2008.
31. Rippon, H.J., Polak, J.M., Qin, M., and Bishop, A.E. Derivation of distal lung epithelial progenitors from murine embryonic stem cells using a novel three-step differentiation protocol. Stem Cells **24,** 1389, 2006.
32. Berger, M.J., Adams, S.D., Tigges, B.M., Sprague, S.L., Wang, X.J., Collins, D.P., and McKenna, D.H. Differentiation of umbilical cord blood-derived multilineage progenitor cells into respiratory epithelial cells. Cytotherapy **8,** 480, 2006.
33. Samadikuchaksaraei, A., Cohen, S., Isaac, K., Rippon, H.J., Polak, J.M., Bielby, R.C., and Bishop, A.E. Derivation of distal airway epithelium from human embryonic stem cells. Tissue Eng **12,** 867, 2006.
34. Van Vranken, B.E., Rippon, H.J., Samadikuchaksaraei, A., Trounson, A.O., and Bishop, A.E. The differentiation of distal lung epithelium from embryonic stem cells. Curr Protoc Stem Cell Biol Chapter 1, Unit 1G 1, 2007.
35. Wang, G., Bunnell, B.A., Painter, R.G., Quiniones, B.C., Tom, S., Lanson, N.A., Spees, J.L., Bertucci, D., Peister, A., Weiss, D.J., Valentine, V.G., Prockop, D.J., and Kolls, J.K. Adult stem cells from bone marrow stroma differentiate into airway epithelial cells: potential therapy for cystic fibrosis. Proc Natl Acad Sci U S A **102,** 186, 2005.
36. Sueblinvong, V., and Weiss, D.J. Stem cells and cell therapy approaches in lung biology and diseases. Transl Res **156,** 188, 2010.
37. Weiss, D.J., and Finck, C. Embryonic stem cells and repair of lung injury. Mol Ther **18,** 460, 2010.

38. Chistiakov, D.A. Endogenous and exogenous stem cells: a role in lung repair and use in airway tissue engineering and transplantation. J Biomed Sci **17,** 92, 2010.
39. Zhang, S., Danchuk, S.D., Imhof, K.M., Semon, J.A., Scruggs, B.A., Bonvillain, R.W., Strong, A.L., Gimble, J.M., Betancourt, A.M., Sullivan, D.E., and Bunnell, B.A. Comparison of the therapeutic effects of human and mouse adipose-derived stem cells in a murine model of lipopolysaccharide-induced acute lung injury. Stem Cell Res Ther **4,** 13, 2013.
40. Danchuk, S., Ylostalo, J.H., Hossain, F., Sorge, R., Ramsey, A., Bonvillain, R.W., Lasky, J.A., Bunnell, B.A., Welsh, D.A., Prockop, D.J., and Sullivan, D.E. Human multipotent stromal cells attenuate lipopolysaccharide-induced acute lung injury in mice via secretion of tumor necrosis factor-alpha-induced protein 6. Stem Cell Res Ther **2,** 27, 2011.
41. Wagner, D.E., Bonvillain, R.W., Jensen, T., Girard, E.D., Bunnell, B.A., Finck, C.M., Hoffman, A.M., and Weiss, D.J. Can stem cells be used to generate new lungs? *Ex vivo* lung bioengineering with decellularized whole lung scaffolds. Respirology **18,** 895, 2013.
42. Ode, A., Duda, G.N., Glaeser, J.D., Matziolis, G., Frauenschuh, S., Perka, C., Wilson, C.J., and Kasper, G. Toward biomimetic materials in bone regeneration: functional behavior of mesenchymal stem cells on a broad spectrum of extracellular matrix components. J Biomed Mater Res A **95,** 1114, 2010.
43. Lindner, U., Kramer, J., Behrends, J., Driller, B., Wendler, N.O., Boehrnsen, F., Rohwedel, J., and Schlenke, P. Improved proliferation and differentiation capacity of human mesenchymal stromal cells cultured with basement-membrane extracellular matrix proteins. Cytotherapy **12,** 992, 2010.
44. Reilly, G.C., and Engler, A.J. Intrinsic extracellular matrix properties regulate stem cell differentiation. J Biomech **43,** 55, 2010.
45. Frith, J.E., Mills, R.J., Hudson, J.E., and Cooper-White, J.J. Tailored integrin-extracellular matrix interactions to direct human mesenchymal stem cell differentiation. Stem Cells Dev **21,** 2442, 2012.
46. Shamis, Y., Hasson, E., Soroker, A., Bassat, E., Shimoni, Y., Ziv, T., Sionov, R.V., and Mitrani, E. Organ-specific scaffolds for *in vitro* expansion, differentiation, and organization of primary lung cells. Tissue Eng Part C Methods **17,** 861, 2011.
47. Guilak, F., Cohen, D.M., Estes, B.T., Gimble, J.M., Liedtke, W., and Chen, C.S. Control of stem cell fate by physical interactions with the extracellular matrix. Cell Stem Cell **5,** 17, 2009.
48. Baber, S.R., Deng, W., Master, R.G., Bunnell, B.A., Taylor, B.K., Murthy, S.N., Hyman, A.L., and Kadowitz, P.J. Intratracheal mesenchymal stem cell administration attenuates monocrotaline-induced pulmonary hypertension and endothelial dysfunction. Am J Physiol Heart Circ Physiol **292,** H1120, 2007.
49. 2011 Annual Report of the U.S. Organ Procurement and Transplantation Network and the Scientific Registry of Transplant Recipients: Transplant Data 1994–2010. Department of Health and Human Services, Health Resources and Services Administration, Healthcare Systems Bureau, Division of Transplantation, Rockville, MD; United Network for Organ Sharing, Richmond, VA; University Renal Research and Education Association, Ann Arbor, MI.
50. Booth, A.J., Hadley, R., Cornett, A.M., Dreffs, A.A., Matthes, S.A., Tsui, J.L., Weiss, K., Horowitz, J.C., Fiore, V.F., Barker, T.H., Moore, B.B., Martinez, F.J., Niklason, L.E., and White, E.S. Acellular normal and fibrotic human lung matrices as a culture system for *in vitro* investigation. Am J Respir Crit Care Med **186,** 866, 2012.
51. Sokocevic, D., Bonenfant, N.R., Wagner, D.E., Borg, Z.D., Lathrop, M.J., Lam, Y.W., Deng, B., Desarno, M.J., Ashikaga, T., Loi, R., Hoffman, A.M., and Weiss, D.J. The effect of age and emphysematous and fibrotic injury on the re-cellularization. Biomaterials **34,** 3256, 2013.
52. Grosse, C., and Grosse, A. CT findings in diseases associated with pulmonary hypertension: a current review. Radiographics **30,** 1753, 2010.
53. Faffe, D.S., and Zin, W.A. Lung parenchymal mechanics in health and disease. Physiol Rev **89,** 759, 2009.
54. Badylak, S.F., Freytes, D.O., and Gilbert, T.W. Extracellular matrix as a biological scaffold material: structure and function. Acta Biomater **5,** 1, 2009.
55. Engler, A.J., Sweeney, H.L., Discher, D.E., and Schwarzbauer, J.E. Extracellular matrix elasticity directs stem cell differentiation. J Musculoskelet Neuronal Interact **7,** 335, 2007.
56. Petersen, T.H., Calle, E.A., Colehour, M.B., and Niklason, L.E. Matrix composition and mechanics of decellularized lung scaffolds. Cells Tissues Organs **195,** 222, 2012.
57. Hoorn, C.M., and Roth, R.A. Monocrotaline pyrrole alters DNA, RNA and protein synthesis in pulmonary artery endothelial cells. Am J Physiol **262,** L740, 1992.
58. Owens, G.K., Rabinovitch, P.S., and Schwartz, S.M. Smooth muscle cell hypertrophy versus hyperplasia in hypertension. Proc Natl Acad Sci USA **78,** 7759, 1981.
59. Crapo, P.M., Gilbert, T.W., and Badylak, S.F. An overview of tissue and whole organ decellularization processes. Biomaterials **32,** 3233, 2011.
60. Nagata, S., Hanayama, R., and Kawane, K. Autoimmunity and the clearance of dead cells. Cell **140,** 619, 2010.
61. Gilbert, T.W., Freund, J.M., and Badylak, S.F. Quantification of DNA in biologic scaffold materials. J Surg Res **152,** 135, 2009.
62. Zheng, M.H., Chen, J., Kirilak, Y., Willers, C., Xu, J., and Wood, D. Porcine small intestine submucosa (SIS) is not an acellular collagenous matrix and contains porcine DNA: possible implications in human implantation. J Biomed Mater Res B Appl Biomater **73,** 61, 2005.
63. Koval, M., Ward, C., Findley, M.K., Roser-Page, S., Helms, M.N., and Roman, J. Extracellular matrix influences alveolar epithelial claudin expression and barrier function. Am J Respir Cell Mol Biol **42,** 172, 2010.
64. Kielty, C.M., Whittaker, S.P., Grant, M.E., and Shuttleworth, C.A. Type VI collagen microfibrils: evidence for a structural association with hyaluronan. J Cell Biol **118,** 979, 1992.
65. Keene, D.R., Engvall, E., and Glanville, R.W. Ultrastructure of type VI collagen in human skin and cartilage suggests an anchoring function for this filamentous network. J Cell Biol **107,** 1995, 1988.
66. Amenta, P.S., Gil, J., and Martinez-Hernandez, A. Connective tissue of rat lung. II: ultrastructural localization of collagen types III, IV, and VI. J Histochem Cytochem **36,** 1167, 1988.
67. Specks, U., Nerlich, A., Colby, T.V., Wiest, I., and Timpl, R. Increased expression of type VI collagen in lung fibrosis. Am J Respir Crit Care Med **151,** 1956, 1995.

68. Aumailley, M., Specks, U., and Timpl, R. Cell adhesion to type-VI collagen. Biochem Soc Trans **19,** 843, 1991.
69. Gimble, J.M., Bunnell, B.A., and Guilak, F. Human adipose-derived cells: an update on the transition to clinical translation. Regen Med **7,** 225, 2012.
70. Gentile, P., Orlandi, A., Scioli, M.G., Di Pasquali, C., Bocchini, I., and Cervelli, V. Concise review: adipose-derived stromal vascular fraction cells and platelet-rich plasma: basic and clinical implications for tissue engineering therapies in regenerative surgery. Stem Cells Transl Med **1,** 230, 2012.
71. Marra, K.G., Brayfield, C.A., and Rubin, J.P. Adipose stem cell differentiation into smooth muscle cells. Methods Mol Biol **702,** 261, 2011.
72. Gaver, D.P., 3rd, and Kute, S.M. A theoretical model study of the influence of fluid stresses on a cell adhering to a microchannel wall. Biophys J **75,** 721, 1998.
73. Sakao, S., Tatsumi, K., and Voelkel, N.F. Endothelial cells and pulmonary arterial hypertension: apoptosis, proliferation, interaction and transdifferentiation. Respir Res **10,** 95, 2009.
74. Huang, C., Bruggeman, L.A., Hydo, L.M., and Miller, R.T. Shear stress induces cell apoptosis via a c-Src-phospholipase D-mTOR signaling pathway in cultured podocytes. Exp Cell Res **318,** 1075, 2012.
75. Wolfe, R.P., and Ahsan, T. Shear stress during early embryonic stem cell differentiation promotes hematopoietic and endothelial phenotypes. Biotechnol Bioeng **110,** 1231, 2013.
76. Zheng, W., Xie, Y., Zhang, W., Wang, D., Ma, W., Wang, Z., and Jiang, X. Fluid flow stress induced contraction and re-spread of mesenchymal stem cells: a microfluidic study. Integr Biol (Camb) **4,** 1102, 2012.
77. Davies, P.F., Spaan, J.A., and Krams, R. Shear stress biology of the endothelium. Ann Biomed Eng **33,** 1714, 2005.
78. Glagov, S., Zarins, C., Giddens, D.P., and Ku, D.N. Hemodynamics and atherosclerosis. Insights and perspectives gained from studies of human arteries. Arch Pathol Lab Med **112,** 1018, 1988.

Address correspondence to:
Bruce A. Bunnell, PhD
Center for Stem Cell Research and Regenerative Medicine
Tulane University School of Medicine
1430 Tulane Avenue, SL-99
New Orleans, LA 70112

E-mail: bbunnell@tulane.edu

Received: July 18, 2013
Accepted: December 2, 2013
Online Publication Date: February 28, 2014